Accurate Analysis of Metamaterials Involving Finite Arrays of Split-ring Resonators and Thin Wires

Levent Gürel[1,2], **Özgür Ergül**[1], **and Alper Ünal**[1]

[1]Department of Electrical and Electronics Engineering, Bilkent University
TR-06800, Bilkent, Ankara, Turkey
[2]Computational Electromagnetics Research Center (BiLCEM), Bilkent University
TR-06800, Bilkent, Ankara, Turkey

Abstract— In order to gain physical insight into how some metamaterial structures behave, we report our results obtained by accurate numerical solutions of electromagnetic problems related to various constructions of split-ring-resonators (SRRs) and thin wires (TWs). Single and multiple layers of arrays of SRRs and TWs are investigated in detail using the electric-field integral equation. Without utilizing any homogenization techniques, we accurately model large numbers of unit cells that translate into very large computational problems, which are solved efficiently by employing multilevel fast multipole algorithm.

1. INTRODUCTION

Since they were first proposed theoretically by Veselago in 1968 [1], metamaterials (MMs) have attracted a great amount of interest because of their unusual electromagnetic properties. MMs are usually constructed by periodical arrangements of unit cells such as split ring resonators (SRRs) and thin wires (TWs). In this paper, we specifically investigate the MM structures consisting of SRR and TW arrays, as depicted in Fig. 1. These two types of arrays are also included in the same medium to obtain composite metamaterials (CMMs). In our modelling and simulations, we take into account that these structures actually have finite extent and they exhibit interface properties. Without using the symmetry and periodicity of these structures, we accurately model large numbers of unit cells to understand their transmission properties. The surfaces are modelled by perfectly conducting sheets and the scattering problems are formulated by the electric-field integral equation (EFIE). With the triangulation of the conducting surfaces, we employ Rao-Wilton-Glisson (RWG) [2] basis functions to expand the unknown surface current density. Accurate modelling of MMs translate into very large computational problems, which can be solved with the aid of advanced acceleration techniques, such as the multilevel fast multipole algorithm (MLFMA) [3].

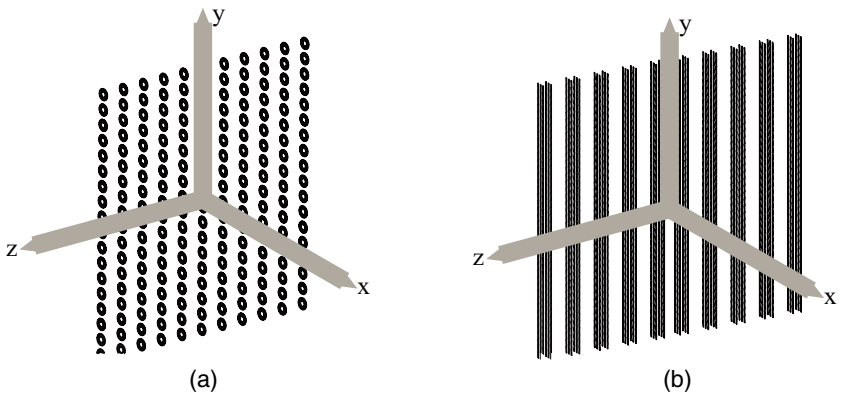

Figure 1: (a) Single-layer SRR array obtained by the arrangement of 11×18 SRRs. (b) TW array having the same dimensions as the SRR array in Fig. 1(a).

In this work, dimensions of the unit cells are in the order of microns to obtain negative effective permeability around 100 GHz [4]. Dimensions of a single SRR are as follows: The smaller ring has 43 μm inner radius and 67.2 μm outer radius, the larger ring has 80.7 μm inner radius and 107.5 μm outer radius, and the gap width is 7.2 μm. The SRR array depicted in Fig. 1(a) is constructed by the arrangement of 11×8 SRRs. Due to the negative effective permittivity stimulated in the medium, the transmission through the array is expected to decrease significantly around the

resonance frequency. Dimensions of the unit cells of the TW array depicted in Fig. 1(b) are compatible with the dimensions of the SRRs and the array exhibits negative effective permittivity in a wide range of frequencies including 100 GHz. As a result, CMM structures obtained by the combination of the SRR and TW arrays in Fig. 1 are expected to show double-negative property around 100 GHz. In this paper, examples on the SRR and CMM arrays are provided to confirm the theoretical findings on practical cases.

2. SIMULATION ENVIRONMENT

In this paper, both the SRR and TW geometries are modelled by open surfaces with zero thickness. Therefore, the scattering problems related to MMs are formulated by EFIE, which is applicable to open geometries. We solve the problems in frequency domain using phasor notation with the e^{-iwt} convention. For conducting surfaces, EFIE can be written as

$$\hat{\boldsymbol{t}} \cdot \int_S d\boldsymbol{r}' \boldsymbol{J}(\boldsymbol{r}') \cdot \left(\bar{\mathbf{I}} - \frac{\nabla\nabla'}{k^2} \right) g(\boldsymbol{r}, \boldsymbol{r}') = \frac{i}{k\eta} \hat{\boldsymbol{t}} \cdot \boldsymbol{E}^{\boldsymbol{i}}(\boldsymbol{r}) \tag{1}$$

directly from the boundary condition for the tangential electric field, where k and η are the wavenumber and wave impedance associated with the host medium. In our simulations, we assume that the relative permittivity of the host medium is 4.8, as it is commonly used in experimental setups [4]. In (1), scattered electric field is expressed in terms of the induced (unknown) surface current $\boldsymbol{J}$ with the aid of the free-space Green's function

$$g(\boldsymbol{r}, \boldsymbol{r}') = \frac{e^{ikR}}{4\pi R} \qquad \left(R = \left| \boldsymbol{r} - \boldsymbol{r}' \right| \right), \tag{2}$$

where $\boldsymbol{r}$ is an observation point on the surface, and $\hat{\boldsymbol{t}}$ is the tangential vector at the observation point. On the right-hand side of (1), $\boldsymbol{E}^{\boldsymbol{i}}(\boldsymbol{r})$ denotes the incident electric field.

For the numerical solutions of EFIE, the unknown current induced on the conducting surfaces is expanded in a series of basis functions $\boldsymbol{b}_n$, i.e.,

$$\boldsymbol{J}(\boldsymbol{r}) = \sum_{n=1}^{N} a_n \boldsymbol{b}_n(\boldsymbol{r}), \tag{3}$$

where a_n represents the unknown coecients for $n = 1, 2, \ldots, N$ and N is the number of unknowns. Then, the application of the method of moments leads to $N \times N$ dense matrix equation

$$\sum_{n=1}^{N} Z_{mn}^{E} a_n = v_m^{E}, \qquad m = 1, \ldots, N, \tag{4}$$

where

$$Z_{mn}^{E} = \int_{S_m} d\boldsymbol{r} \boldsymbol{t}_m(\boldsymbol{r}) \cdot \int_{S_n} d\boldsymbol{r}' \left(\bar{\mathbf{I}} - \frac{\nabla\nabla'}{k^2} \right) g(\boldsymbol{r}, \boldsymbol{r}') \cdot \boldsymbol{b}_n(\boldsymbol{r}') \tag{5}$$

represents the matrix element, and

$$v_m^{E} = \frac{i}{k\eta} \int_{S_m} d\boldsymbol{r} \boldsymbol{t}_m(\boldsymbol{r}) \cdot \boldsymbol{E}^{\boldsymbol{i}}(\boldsymbol{r}) \tag{6}$$

represents the mth element of the excitation vector. We apply the Galerkin scheme by choosing the testing functions t_m also as RWG. In (5) and (6), S_m and S_n symbolize the spatial supports of the mth testing and nth basis functions, respectively.

The matrix equation in (4) is solved iteratively, where the matrix-vector products are accelerated by MLFMA. The fundamental idea in MLFMA is to replace the element-to-element interactions with cluster-to-cluster interactions in a multilevel scheme. This computational scheme relies on the factorization of the Green's function, which is valid only for basis and testing functions that are far from each other. By employing MLFMA, matrix-vector multiplications can be performed in $O(N \log N)$ processing time using $O(N \log N)$ memory as detailed in [5].

EFIE usually produces ill-conditioned matrix equations that are dicult to solve by an iterative algorithm [6]. In addition, MM structures usually present numerical resonances, which further

inhibits a quick convergence without preconditioning. To obtain a convergence in a reasonable number of iterations, we employ near-field preconditioner (NFP) obtained by retaining all of the available near-field interactions. NFP is not commonly used in the solutions of large scattering problems, since it has a complexity larger than MLFMA. However, for all problems investigated in this work, we observe that the additional time required for the factorization and use of NFP is smaller than the time gained by the reduction of the iterations. In addition to NFP, we also employ more robust and efficient preconditioners based on approximate MLFMA inserted in flexible solvers consisting of inner and outer iterations.

3. RESULTS

Figure 2 presents the results for the SRR array in Fig. 1(a), where the power transmission is plotted at various frequencies, i.e., 95 GHz, 100 GHz, and 110 GHz. The transmission is calculated at different points in the $z = 0$ plane and the SRR arrays are depicted in the plots. The excitation is a Hertzian dipole oriented in the y direction as also indicated in the plots and the transmission region is on the left of the arrays. At 95 GHz and 105 GHz, the power transmission through the 1-layer SRR array is almost unity, which corresponds to 0 decibels (dB). On the other hand, around the resonance frequency (100 GHz), the transmitted power drops dramatically due to the shadowing effect of the SRR array. In other words, negative effective permeability is stimulated in the medium at 100 GHz. In the 2-layer case, the frequency range for the resonance effect is extended and the transmitted power is slightly blocked also at 95 GHz and 105 GHz.

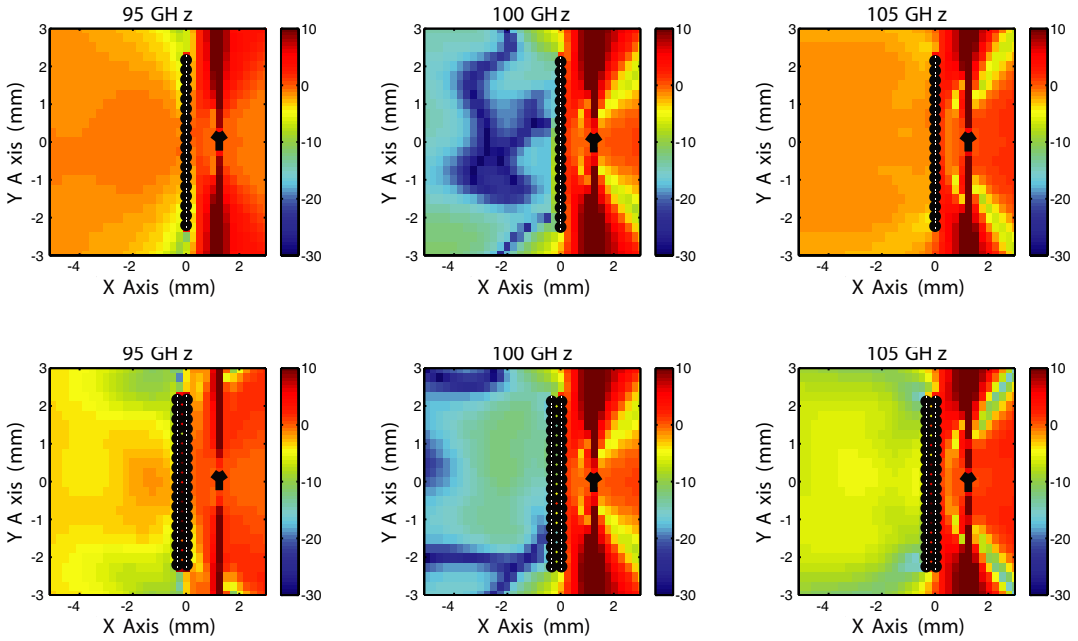

Figure 2: Power transmission for the 1-layer and 2-layer 11 × 18 SRR arrays at 95 GHz, 100 GHz, and 105 GHz. SRRs and the ideal (Hertzian) dipole are also depicted in the figures and the transmission region is on the left of the array.

Figure 3 presents the power transmission for the 1-layer and 2-layer CMM arrays constructed by employing the SRR and TW arrays in Fig. 1. At 95 GHz and 105 GHz, we observe that the array blocks the fields and this is mainly due to the negative effective permittivity introduced by the TWs. On the other hand, the transmission through the CMM array increases at 100 GHz, which is more visible in the 2-layer case. The reason is that the SRRs resonate around 100 GHz as depicted in Fig. 2. Then, both the effective permittivity and permeability stimulated in the medium become negative. We note that increasing the number of layers provides an extended range for the negative effective permeability introduced by the SRRs and this leads to increased double-negativity effect, i.e., more power transmission around the resonance frequency, obtained from the CMM structure.

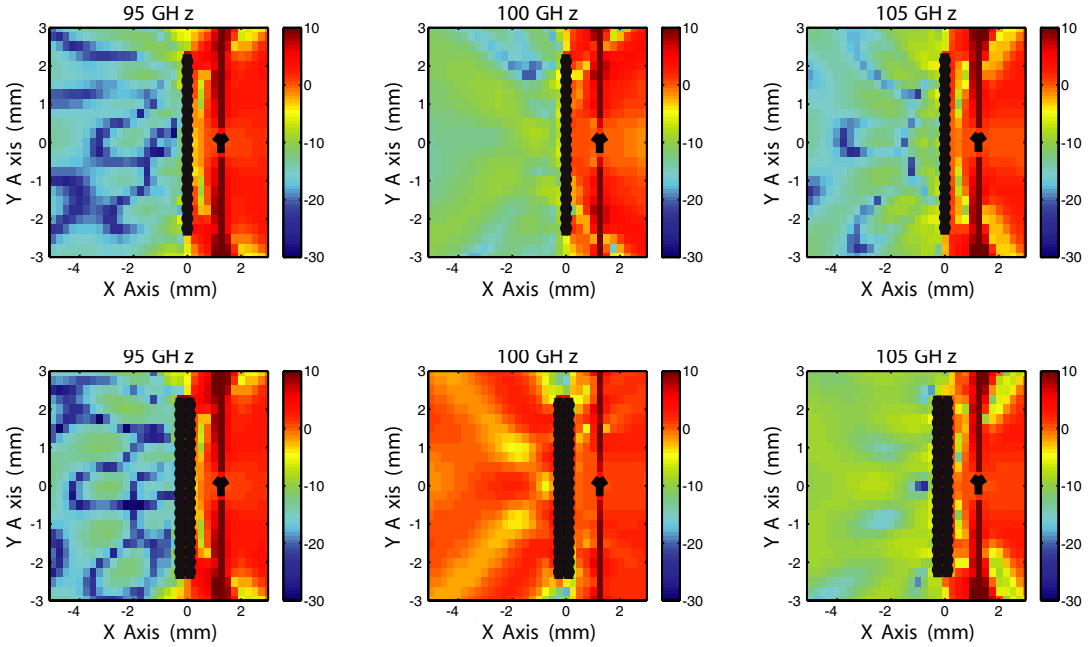

Figure 3: Power transmission for the 1-layer and 2-layer CMM arrays at 95 GHz, 100 GHz, and 105 GHz. The arrays and the ideal (Hertzian) dipole are also depicted in the figures and the transmission region is on the left of the arrays.

ACKNOWLEDGMENT

This work was supported by the Scientific and Technical Research Council of Turkey (TUBITAK) under Research Grant 105E172, by the Turkish Academy of Sciences in the framework of the Young Scientist Award Program (LG/TUBA-GEBIP/2002-1-12), and by contracts from ASELSAN and SSM.

REFERENCES

1. Veselago, V. G., "The electrodynamics of substances with simultaneously negative values of permittivity and permeability," *Sov. Phys. Usp.*, Vol. 10, No. 4, 509–514, 1968.
2. Rao, S. M., D. R. Wilton, and A. W. Glisson, "Electromagnetic scattering by surfaces of arbitrary shape," *IEEE Trans. Antennas Propagat.*, Vol. AP-30, No. 3, 409–418, 1982.
3. Lu, C.-C. and W. C. Chew, "Multilevel fast multipole algorithm for electromagnetic scattering by large complex objects," *IEEE Trans. Antennas Propagat.*, Vol. 45, No. 10, 1488–1493, 1997.
4. Gokkavas, M., K. Güven, I. Bulu, K. Aydın, R. S. Penciu, M. Kafesaki, C. M. Soukoulis, and E. Özbay, "Experimental demonstration of a left-handed metamaterial operating at 100 GHz," *Phys. Rev. B.*, Vol. 73, No. 193103, 2006.
5. Chew, W. C., J.-M. Jin, E. Michielssen, and J. Song, *Fast and Efficient Algorithms in Computational Electromagnetics*, Artech House, Boston, MA, 2001.
6. Gürel, L. and Ö. Ergül, "Comparison of FMM implementations employing different formulations and iterative solvers," *2003 IEEE AP-S International Symposium*, Columbus, Ohio, Vol. 1, 19–22, June 2003.